PHYSICAL REVIEW B

CONDENSED MATTER

THIRD SERIES, VOLUME 39, NUMBER 13 1 MAY 1989

Optical-absorption and photoionization measurements from the excited states of Ce^{3+}:$Y_3Al_5O_{12}$

D. S. Hamilton, S. K. Gayen,* G. J. Pogatshnik,† and R. D. Ghen‡
Department of Physics and Institute of Materials Science, University of Connecticut, Storrs, Connecticut 06269-3046

W. J. Miniscalco
GTE Laboratories, Incorporated, 40 Sylvan Road, Waltham, Massachusetts 02254
(Received 5 December 1988)

The optical transitions in Ce^{3+}:$Y_3Al_5O_{12}$ from the lowest $5d$ excited state of the Ce^{3+} ion to the host conduction band have been investigated. Two spatially overlapped and time-sequenced laser pulses were used to observe directly the excited-state absorption (ESA) and the two-step photoionization of the cerium ions. The peak cross section of the ESA transition is $(1.0\pm0.3)\times10^{-17}$ cm^2 at 700 nm. The ESA spectrum was measured from 600 to 880 nm and is used to construct an energy-level diagram for the Ce^{3+} ions relative to the energy-band states of the $Y_3Al_5O_{12}$ host. The energy gap between the lowest relaxed $5d$ state and the conduction-band edge is estimated to be 10 000 cm^{-1}. Strong-probe saturation measurements indicate a slow and inefficient back-transfer of excitation to the cerium ions following the ESA. Photoconductivity measurements were used to confirm the two-step photoionization of the cerium ions.

I. INTRODUCTION

When an excited electronic state of a system is significantly populated, it is possible to observe optically induced transitions which originate from this excited state. These transitions can involve either stimulated emission or absorption, depending on the optical frequency and the energy-level structure of the system. Measurements of excited-state-absorption (ESA) spectra provide important characteristics of the higher-lying energy states which are not evident from absorption measurements originating in the ground state. ESA is also an important potential-loss mechanism for solid-state laser materials if the ESA spectrum overlaps the emission spectrum. The possibilities for such an overlap are enhanced in materials with spectrally broad emission and absorption bands characteristic of vibronic wavelength-tunable lasers. ESA can have a detrimental effect on the laser performance of these materials by reducing the gain and narrowing the tuning range. An extreme case of the deleterious role of ESA is Ce^{3+}:$Y_3Al_5O_{12}$ (YAG), where the ESA is sufficiently strong to completely quench any possible laser action.[1–3] The crystal shows a net optical loss instead of optical gain at the wavelengths of the fluorescence transition.

Figure 1 illustrates the ground-state optical-absorption spectrum of Ce^{3+}:YAG where an undoped YAG sample was used to remove any features which are not due to the Ce^{3+} ions. The spectrum shows the intense parity-allowed $4f\rightarrow5d$ transitions of the Ce^{3+} ions superimposed on a rising background absorption. In previous measurements[1–3] of the ESA in Ce^{3+}:YAG, the cerium ions were excited to the second $5d$ level, which peaks at about 340 nm. A rapid intraconfigurational relaxation leaves the electron in the lowest $5d$ state which served as an initial state for the ESA. By employing a wavelength-tunable probe beam which is absorbed by the excited cerium ions, the strength of the ESA transition has been observed to increase monotonically with increasing probe wavelength over the range 500–680 nm. On the basis of the size of the ESA cross section, it has been suggested[3] that the ESA transition terminates in the YAG conduction band.

In the present work we will use the results from several experiments to demonstrate that a photoionization transition from the lowest $5d$ Ce^{3+} level to the YAG conduction band is responsible for the strong ESA transition in this material and explore the implications of this two-step photoionization. Recent photoconductivity measurements[4] in Ce^{3+}:YAG have determined a 3.8-eV threshold energy for the Ce^{3+} $4f$ ground-state to conduction-band one-photon-photoionization transition. This energy corresponds to an optical excitation wavelength of 326 nm. With this value in mind, we will present measurements of

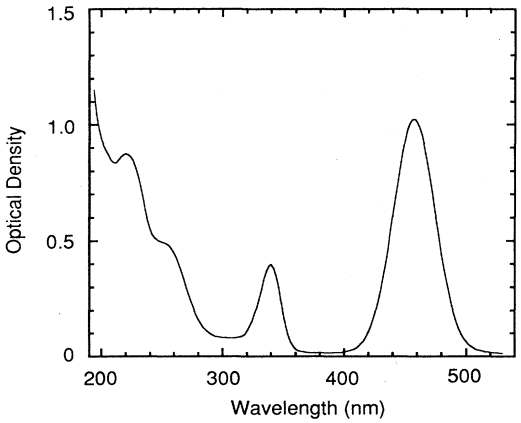

FIG. 1. The ground-state absorption spectrum of Ce^{3+}:YAG taken with a dual-beam spectrophotometer using an undoped YAG sample in the reference arm.

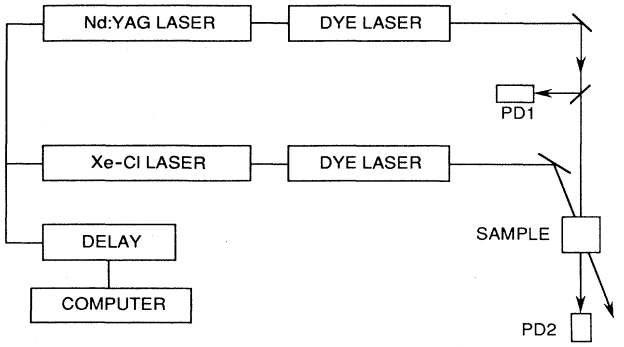

FIG. 2. Diagram of the experimental apparatus for measuring excited-state absorption.

the ESA in Ce^{3+}:YAG following both 500-nm and 308-nm pumping. The 500-nm excitation wavelength is well below the photoionization threshold and into the low-energy tail of the $4f$ to lowest-$5d$ absorption band. In this case we observe a single ESA transition which originates on this $5d$ level. For the 308-nm pumping, which is above the photoionization threshold, multiple transient absorptions are observed. These transient absorptions involve both the Ce^{3+} ions and longer-lived color centers produced following the photoionization of the cerium ions.

The spectral dependence of the ESA on the probe wavelength has been extended out to 880 nm. This has allowed us to locate the peak of the ESA spectrum and estimate the gap between the lowest relaxed $5d$ state and the conduction-band edge. The spectral band shape and the magnitude of the ESA cross section are characteristic of a photoionization transition. Using an intense probe beam which partially saturates the ESA transition, we have observed a slow and inefficient recombination of the photoelectrons and cerium ions in the excited cerium states. The two-step photoionization of the Ce^{3+} ions was also observed directly using a photoconductivity cell and two time-sequenced laser beams.

II. EXPERIMENTAL APPARATUS

The experimental apparatus used for the ESA measurements is illustrated schematically in Fig. 2. The excitation source for populating the lowest-$5d$ level was a tunable dye laser pumped by a 308-nm Xe-Cl excimer laser (Quanta-Ray EXC-1). The dye-laser output had a 0.1-cm^{-1} bandwidth and a 5-nsec duration. This pump beam was focused to a 1.0-mm nominal-diameter spot on the sample by a 35-cm-focal-length fused-silica lens. A beam splitter directed a small fraction of the beam to a Joulemeter to monitor the energy per pulse of the pump beam. The pump-beam energy at the sample was typically 0.12 mJ. At a wavelength of 500 nm, the excitation was into the low-energy tail of the lowest $4f \rightarrow 5d$ absorption where the ground-state absorption coefficient was measured to be $\alpha = 9.0\ cm^{-1}$. Excitation at this wavelength results in a minimal thermal loading of the crystal and a convenient penetration depth of the pump beam. By placing an additional mirror at the excimer-laser output, we were also able to pump into the high-energy tail of the second $5d$ level with the 308-nm beam.

A second dye laser, pumped by the second harmonic of a Nd:YAG laser (Quanta-Ray DCR-1) generated the probe beam. The probe beam, which had similar spectral and temporal characteristics as the pump beam, was focused by a 50-cm-focal-length achromat to a 0.4-mm-diameter spot concentric with the pump-beam spot. The crossing angle between the pump and probe beams was approximately 2°. Neutral density filters were used to reduce the probe-beam energy at the sample to about 5 nJ for the ESA measurements in order not to disturb the excited-state population. The probe-beam intensity was monitored with a beam splitter and photodiode combination before the sample and the transmitted probe-beam intensity was detected by an identical photodiode placed behind the sample. Depending on the wavelength of the probe beam, different glass cutoff filters were placed between the sample and the photodiode to block the pump-beam-induced cerium fluorescence from the detector.

To set the time delay between the arrival of the pump and the probe beams at the sample, the lamp-output strobe from the Nd:YAG laser was delayed by 240 μsec and then used to simultaneously trigger two Canberra 2055 time-delay generators. One of these provided the external trigger pulse to the Q switch of the Nd:YAG laser. The other delay generator was used to trigger a computer-controlled, programmable, time-delay generator (Evans 4145-2) which could be digitally incremented in 10-nsec intervals over a 100-μsec range. The output from this delay generator was then used to trigger the excimer laser. A reference setting for the relative time delay between the pump and probe laser pulses was set by placing a 1P28 photomultiplier just in front of the sample and observing the light pulses as displayed on a 50-Ω-terminated oscilloscope. The time-delay generators were then adjusted for proper sequencing of the laser pulses.

The rms jitter in the time interval between the two pulses was about 2 nsec. A laser repetition rate of 10 pulses per second was maintained throughout the experiment.

An Apple II microcomputer was interfaced to read the signal and reference photodiode outputs via two 12-bit analog-to-digital converters. To account for any residual pump-induced fluorescence or scattered laser light detected by the photodiodes, a computer-controlled electromechanical shutter was used to block the probe beam while the computer recorded the background levels. Short-term random fluctuations and wavelength-dependent variations in the probe-beam intensity were corrected for by taking the ratio of the transmitted probe signal to the output of the reference photodiode. To achieve an adequate signal-to-noise ratio, this normalized probe transmission was averaged over 100 laser shots. The kinetics of the transient absorption were measured by repetitively recording this averaged probe transmission and then incrementing the programmable delay generator to a new delay value. In addition, the normalized probe transmission was measured when the probe beam preceded the pump beam by about 40 nsec and when the pump beam was blocked with a second computer-controlled shutter.

To observe the partial saturation of the ESA transition and the subsequent recovery of the population of the lowest-$5d$ level, the neutral density filters were changed so that the 500-nm-pump-beam energy was reduced to 100 nJ and the probe-beam energy was increased to 1.1 mJ. In addition, the pump and probe beams were refocused to 0.3-mm and 0.4-mm spot diameters, respectively. The emission, which was proportional to the Ce^{3+} population in the lowest-$5d$ state, was monitored using a $\frac{1}{2}$-m spectrometer tuned to the 560-nm peak of the $5d \rightarrow 4f$ fluorescence. The output of the photomultiplier tube at the exit slit could be displayed on an oscilloscope to measure the time dependence of the emission or recorded by a Keithley 610C electrometer to determine the time-averaged values.

The sample cell for the photoconductivity measurements was of a blocking electrode design[5] where the electrodes are not in direct contact with the sample. The front electrode was a 2.5×2.5-cm^2 fused-silica plate with a semitransparent metallic coating. A 0.5-mil-thick, fused-silica, cover slip was sandwiched between the metallic coating and the sample. A second fused-silica cover slip was placed between the sample and the rear copper-foil electrode. Typical electric field strengths were 2000 V/cm. Details of the cell design have been presented elsewhere.[6] The two-step photoconductivity was measured using two dye lasers pumped by the second and third harmonics of a Nd:YAG laser. The first dye laser was operated at 460 nm, which corresponds to the peak of the $4f$ to lowest-$5d$ absorption. The second dye-laser beam with a 700-nm wavelength was delayed by 10 nsec with respect to the arrival of the first dye-laser pulse. The resulting photocurrent was measured by a Keithley 610C electrometer.

The 0.5 mol % Ce^{3+}:YAG samples used were grown by Airtron Inc. using the Czochralski technique. For the ESA measurements, a polished $3 \times 3 \times 6$ mm^3 sample was used with a 3-mm absorption path length. The photoconductivity measurements were done with a 6-mm diameter by 0.15-mm-thick, disk-shaped sample.

III. ANALYSIS METHODS

The excited-state absorption coefficient α^* depends on the concentration of excited cerium ions which can interact with the probe beam as it travels through the sample. This concentration is proportional to the energy density deposited in the sample by the pump beam. In this section we derive the relationship between the pump- and probe-beam parameters and show how the ESA cross section can be determined from the measured excited-state absorption coefficient. These results are then used to find an expression for the response of the photoconductivity cell for the two-step photoionization.

The pump beam can be described by a photon flux $F(x,y,z,t)$ in photons cm^{-2}sec^{-1} moving down the z axis. Assuming that the confocal parameter of the focus is large compared to the sample length L, the flux can be written as $F=N(z)J(x,y)S(t)$, where the number of photons in the beam is described by N, and J and S are unity-normalized, transverse-spatial, and temporal profiles of the beam, respectively. If the characteristic time duration of the pump pulse is short compared to lifetime τ of the single state which is excited by the pulse at $t=0$, then the excited-state ion concentration can be written as

$$c(x,y,z,t)=\alpha\beta N(z)J(x,y)e^{-t/\tau} , \tag{1}$$

where α is the ground-state absorption coefficient at the pump wavelength and β is the pumping quantum efficiency. We have assumed there is no saturation due to the pump pulse and that Beer's law, $dF=-\alpha F\,dz$, describes the change in the pump flux in an infinitesimal length dz. Thus, if $N(0)$ is the number of incident pump photons, the concentration of excited-state ions can be expressed as

$$c(x,y,z,t)=\alpha\beta N(0)J(x,y)e^{-\alpha z}e^{-t/\tau} . \tag{2}$$

The probe beam, whose flux is described by $f=n(z)j(x,y)s(t)$, is absorbed by the excited-state ions, but not the ions in the ground state. The change in the probe flux in a length element dz due to this absorption is

$$df=-\sigma^* c(x,y,z,t')j(x,y)n(z)dz , \tag{3}$$

where the probe pulse at time t' has a duration short compared to τ, and σ^* is the excited-state absorption cross section per ion. We have assumed that σ^* is much larger than the stimulated-emission cross section in the wavelength region of interest. Substituting Eq. (2) into Eq. (3) and then integrating over the transverse coordinates x and y, we have

$$dn(z)=-\sigma^* N(0)e^{-t'/\tau}W\alpha\beta e^{-\alpha z}n(z)dz , \tag{4}$$

where W is the overlap integral of the pump and probe profiles,

$$W=\int\int_{-\infty}^{\infty} j(x,y)J(x,y)dx\,dy . \tag{5}$$

Equation (4) can then be integrated down the sample of length L to yield

$$\alpha^* L = \ln\left[\frac{n(0)}{n(L)}\right] = \sigma^* N(0) e^{-t'/\tau}(1-e^{-\alpha L})\beta W \ , \quad (6)$$

where $n(0)$ and $n(L)$ are the number of incident and transmitted probe photons, respectively.

We have used this same coaxial beam geometry for the two-step photoconductivity measurements. An equation for the photoresponse can be derived for a cell which utilizes a pair of blocking electrodes. Viewing the sample as a dielectric material placed within a parallel-plate capacitor, the induced polarization surface charge at the electrodes per laser pulse is $\Delta Q = A\,\Delta P$, where A is the sample cross-sectional area and P is the magnitude of the sample polarization. The change in the polarization can be related to the change in the number of photoinduced dipoles by

$$\Delta P = \frac{\Delta n_d \langle p \rangle}{AL} \ , \quad (7)$$

where Δn_d is the number of dipoles created by the two-step laser excitation and $\langle p \rangle$ is their average dipole moment. The average dipole moment can be written as

$$\langle p \rangle = e\omega = e\omega_0 E \ , \quad (8)$$

where ω is the *Schubweg* or average range of the electrons, ω_0 is the *Schubweg* per unit field and E is the electric field strength between the plates. We have assumed that ω is much less than the sample thickness L. Following an ESA transition which photoionizes a cerium ion, the electron can either remain at the cerium site or can migrate away to form the dipole. To account for the two possibilities, we define a quantum efficiency for the photoproduction of dipoles as $\eta = \Delta n_d / \Delta n$, where Δn is the number of photons absorbed from the second laser pulse. Thus the number of dipoles created per laser pulse pair is

$$\Delta n_d = \eta \Delta n = \eta n(0)(1-e^{-\alpha^* L}) \ , \quad (9)$$

where α^* is the ESA coefficient of Eq. (6). We can then combine Eqs. (7)–(9) to give an expression for the induced charge on the electrodes per laser pulse pair as

$$\Delta Q = \frac{\eta n(0)}{L}(1-e^{-\alpha^* L}) e\omega_0 E \ . \quad (10)$$

IV. EXPERIMENTAL RESULTS

The instantaneous density of excited cerium ions and, hence, the ESA coefficient α^* depends on the lifetime of the electronic state from which the ESA transition originates. To determine this lifetime, we have measured the ESA coefficient as a function of the pump-to-probe time delay. The results of this measurement for 500-nm pumping are shown in Fig. 3. Each data point represents the natural logarithm of the ratio of the probe transmission measured when the probe pulse precedes the pump pulse by 40 nsec to the probe transmission at the given delay. This method of normalization was found to be equivalent to fixing the baseline from the probe transmission when the pump beam was blocked. The decay of the ESA coefficient is seen to be exponential with a 68±5-nsec single decay time. This decay time for the ESA is nearly identical to the 64±2-nsec fluorescence lifetime of the lowest-5d state in Ce^{3+}:YAG measured by pumping at 500 nm and the 65-nsec value reported by Weber.[7] This indicates that the single initial level of the ESA transition is the same lowest-5d state of the Ce^{3+} ion.

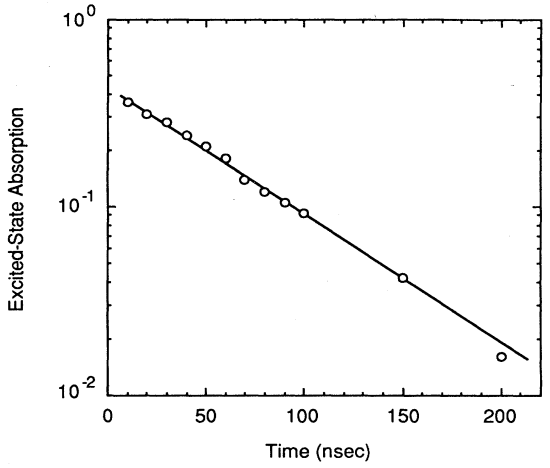

FIG. 3. Decay of the excited-state absorption $\alpha^* L$ as a function of the 500-nm pump to 680-nm probe pulse delay. The straight line is a fit to an exponential with a 68-ns decay constant.

In contrast to the exponential time decay of the ESA coefficient following 500-nm pumping, the ESA kinetics for 308-nm pumping, which is displayed in Fig. 4, are nonexponential. The initial decay of the ESA shows the same 68-nsec lifetime component as before. But at delays

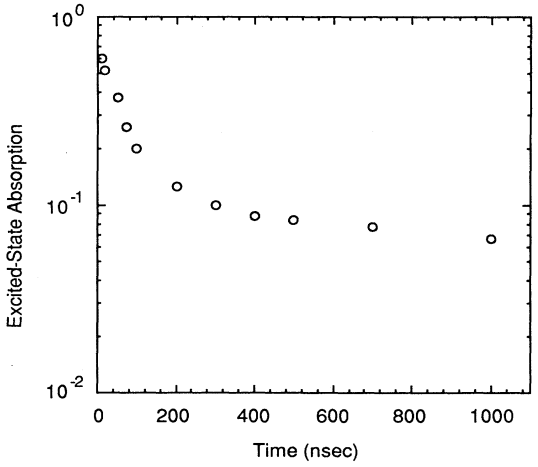

FIG. 4. The multicomponent decay of the excited-state absorption $\alpha^* L$ for 308-nm pumping.

greater than about 100 nsec, the decay curve becomes noticeably nonexponential and develops a component with a much longer decay time. Similar results for the room-temperature kinetics of the ESA coefficient have been noted for 350-nm (Ref. 1) and 337-nm pumping[8] and for the Ce^{3+} photoluminescence with 266-nm pumping.[9] These multicomponent decay curves indicate that additional configurations such as transient color centers are involved when the sample is pumped with these shorter wavelengths.

To verify that the ground-state absorption was not being saturated by the pump pulse and to rule out any significant multiphoton excitations, we have measured the ESA coefficient as a function of the pump energy per pulse. The results of this measurement for 500-nm excitation show a simple linear relationship[10] in agreement with Eq. (6). A similar dependence is observed for 308-nm pumping for both the 70 nsec and long-term transient absorptions.

We have measured the ESA coefficient with 500-nm pumping as a function of the probe wavelength between 600 and 880 nm. Four different dyes (Exciton Chemical: DCM, LDS 750, LDS 751, and LDS 821) were used to produce the composite spectrum displayed in Fig. 5. For spectrally adjacent dyes, data points were taken at overlapping wavelengths to find the near unity scale factors needed to account for the small alignment and overlap variations due to the dye changes. The ESA spectrum is seen to rise monotonically from 600 to 680 nm as has been previously measured,[1-3] peaks at approximately 700 nm, and then falls steadily with increasing wavelength. The spectral dependence of the ESA transition at shorter wavelengths as measured by Miniscalco *et al.*[2] has been scaled to match the 660-nm data point and is also shown in Fig. 5.

The ESA cross section σ^* can now be calculated from Eq. (6). Evaluation of the transverse overlap integral is fully discussed in the Appendix. Assuming a pumping quantum efficiency β of unity, the ESA cross section at a probe wavelength of 700 nm is estimated as $(1.0\pm0.3)\times10^{-17}$ cm^2 for 500-nm pumping and $(1.7\pm0.4)\times10^{-18}$ cm^2 for 308-nm pumping. The difference between these two values can be accounted for if the value of β for 308-nm pumping is 0.17 instead of 1.0. This reduced value of β for the uv pumping would suggest that energy states in addition to the lowest-5*d* state of the Ce^{3+} ions are being excited by these shorter pump wavelengths.

The oscillator strength for the ESA transition was found by numerically integrating the cross section over the ESA band from $\tilde{\nu}=11\,400$–$21\,800$ cm^{-1}. Using

$$f=(1.13\times10^{12})\frac{9n}{(n^2+2)^2}\int\sigma(\tilde{\nu})d\tilde{\nu}\ , \tag{11}$$

where the index of refraction of YAG at 700 nm is $n=1.83$, the oscillator strength f is estimated to be approximately 0.03. Since we have only a part of the full ESA band in Fig. 5, the total oscillator strength will be somewhat larger than this estimate.

To provide additional insight into the photoionization processes involved in the ESA transition, we have used a strong probe beam to partially saturate this absorption. By removing the neutral density filters in the probe beam and increasing the power of the Nd:YAG laser, the 680-nm probe beam was made sufficiently intense so as to significantly alter the population of the lowest-5*d* state. The depopulation of the lowest-5*d* state was evident from the sudden drop of the $5d\rightarrow4f$ fluorescence concurrent with the arrival of the saturating probe pulse as illustrated in Fig. 6. Using the experimental parameters noted in Sec. II, we observed an approximate 70% drop in the fluorescence signal immediately following the 10-nsec probe pulse. After the probe pulse, the Ce^{3+} fluorescence does not recover to its prepulse value but instead continues to drop with a 68-nsec lifetime, reflecting the reduced

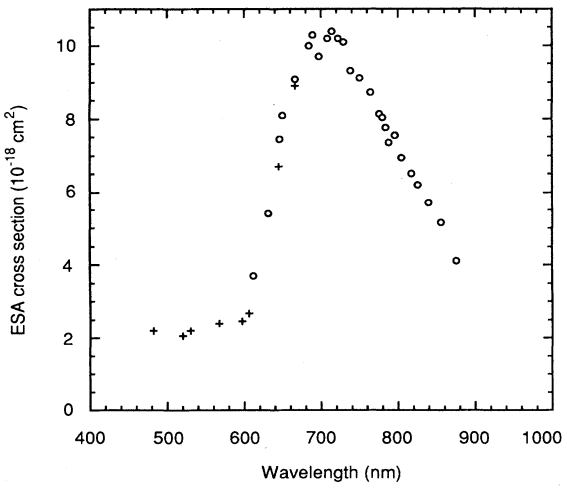

FIG. 5. Wavelength dependence of the excited-state cross section σ^*. The open circles are the values measured in this work, the plus (+) signs are the scaled values from Miniscalco *et al.* (Ref. 2).

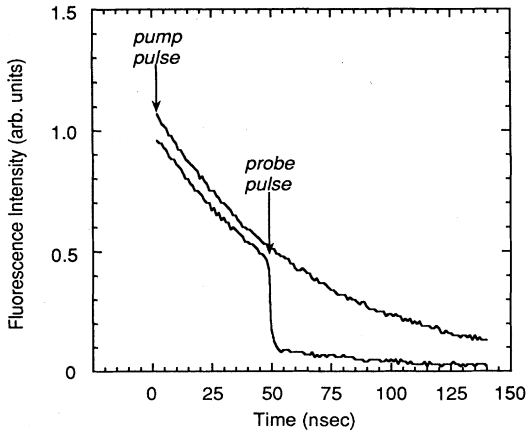

FIG. 6. Decay of the lowest-5*d* state in Ce^{3+}:YAG. The upper trace shows the decay following pulsed excitation at 500 nm. The lower trace shows the depopulation of the 5*d* state due to a strong 700-nm probe pulse at a 50-nsec time delay.

population remaining in the lowest-$5d$ state. Moreover, at much later times, the fluorescence decay becomes nonexponential and develops a long tail with a limiting lifetime of order 10 μsec. This long lifetime tail is observed only in the presence of both the pump and the strong saturating probe, and falls in strength with increasing pump-to-probe delay and decreasing pump or probe intensity. The spectrum of this long lifetime emission is the same as that for the lowest-$5d$ level. This delayed phosphorescence or afterglow is thus the result of a slow back-transfer of excitation into the Ce^{3+} $5d$ levels.

To determine the efficiency of this back-transfer process, we have measured the time average of the $5d \rightarrow 4f$ fluorescence over a number of laser pulses by replacing the oscilloscope by a Keithley electrometer. This time-averaged fluorescence has a maximum when the probe pulse precedes the pump pulse, drops by 60% to a minimum value when the pump-to-probe delay is approximately 5 nsec and then increases back toward the maximum value at longer delays. This implies that 40% is an upper limit for the back-transfer efficiency to the excited state. The remaining excitation presumably returns directly to the Ce^{3+} ground state.

The photoconductivity measurements were done using either one or two pulsed laser beams to illuminate the sample. Using a single 460-nm laser beam with a 1-mJ/cm^2 per pulse fluence and a 10-Hz repetition rate, the resulting photocurrent was approximately at the minimum detectable value of 5×10^{-15} A. With a 700-nm wavelength single beam at 1 mJ/cm^2, no detectable photocurrent was observed. However, when both beams were present with a 10-nsec delay in the arrival of the 700-nm pulse with respect to the 460-nm pulse, a photocurrent of 4×10^{-14} A was observed. The 460-nm wavelength is at the peak of the lowest-$5d$ absorption and the 700-nm corresponds to the peak of the ESA spectrum. This photocurrent, which is observed when both beams impinge upon the sample, is due to the two-step photoionization of the cerium ions. Continued illumination of the sample in an electric field produced a significant permanent dipole moment. Thermal annealing of the sample quenched this moment by recombining the trapped electrons with the cerium hole centers.

By using a tighter focus on the 460-nm beam to increase the per pulse fluence to 2 mJ/cm^2, a 2×10^{-14}-A photocurrent was measured, while only this single beam was used to illuminate the sample. We have interpreted this result as being due to the ESA at 460 nm. That is, two photons from the single 460-nm beam promoted the electron from the cerium ground state to the conduction band in a stepwise process. Due to the low values of the photocurrent, flux dependent measurements did not conclusively show the expected quadratic behavior. Nevertheless, the size of the photocurrent approximately agrees with that predicted from the ratio of the ESA cross sections at 460 and 700 nm.

A much larger photocurrent was observed when the third harmonic of the Nd:YAG laser at 355 nm was used as the excitation source. At this wavelength the excitation was into the region of the second $5d$ absorption band of the cerium ions. At a 100-mJ/cm^2 fluence, a 2×10^{-12}-A photocurrent was measured. The flux-dependence data, taken between 10 and 100 mJ/cm^2 showed a linear relationship.[6] Thus, the origin of this photocurrent for the shorter-wavelength pumping is the direct one-step photoionization of the cerium ions.

V. DISCUSSION

The kinetics of the ESA transition for the 500-nm pumping show a single 70-nsec decay time, identical to the radiative lifetime of the lowest-$5d$ state. This equivalence identifies the lowest-$5d$ state as the single initial state of the ESA transition. The terminal state of the ESA is more difficult to uniquely identify. The large oscillator strength ($f > 0.03$) seems to rule out an ESA transition between crystal-field-split states of the $5d$ electron, due to parity considerations. In addition, if we add the energy of the no-phonon transition to the lowest-$5d$ state (20 440 cm^{-1}) measured by Robbins[11] to the energy corresponding to the peak of the ESA (14 300 cm^{-1}), the terminal state of the ESA transition would be expected to show up as a peak in the ground-state absorption spectrum at 34 740 cm^{-1}. However, there is no peak in the ground-state absorption spectra within 5000 cm^{-1} of this value.

Although more localized charge-transfer transitions have oscillator strengths comparable to the value we have measured for the ESA transition, the results of the strong-probe saturation and recovery experiment are more consistent with the ESA terminating on a state with a much more diffuse wave function and a higher electron mobility. The probe-induced, microsecond-lifetime tail on the $5d \rightarrow 4f$ fluorescence indicates that the $5d$ state is being repopulated from a metastable configuration which is coupled to the terminal state of the ESA. Such a tail is similar to the $5d \rightarrow 4f$ microsecond afterglow phosphorescence of Ce^{3+}:YAG observed under cathode-ray excitation.[12] This room-temperature afterglow results from electrons trapped at the various intrinsic defect sites in the crystal being thermally excited into the conduction band and recombining with the cerium ions. For an ESA transition originating from the lowest-$5d$ state and terminating in the conduction band, the wave function of the terminal state would then be sufficiently diffuse to overlap these intrinsic trap sites. The electrons populating these diffuse carrier states will either rapidly retrap at the hole at the cerium site or populate one of the intrinsic electron traps of the YAG lattice. With a strong probe pulse, a sufficiently large population at the trap sites can be created and the subsequent thermally activated back-transfer to the cerium sites results in the observed afterglow phosphorescence.

An extrapolation on the low-energy side of the ESA spectrum of Fig. 5 predicts that the conduction-band edge lies about 10 000 cm^{-1} above the relaxed lowest-$5d$ level. If we add this energy to the 20 440 cm^{-1} between the $4f$ ground state and the relaxed lowest-$5d$ level,[11] we would predict a photoionization threshold for transitions originating on the $4f$ state of about 30 440 cm^{-1}. This value is in excellent agreement with the ground-state photoconductivity results[4] of a 30 650 cm^{-1} (3.8 eV)

threshold. This relationship between the energies of the cerium levels and the band states of the YAG host is illustrated in Fig. 7. The valence-band to conduction-band gap[13] is 50 000 cm^{-1}. The positions of the bottom of the two lowest-5*d* levels relative to the 4*f* ($^2F_{5/2}$) state are fixed from the measured no-phonon transition energies.[11] The conduction-band edge is seen to overlap the position of the second 5*d* level. Thus the wave functions describing the states at energies higher than the conduction-band edge involve a superposition of delocalized Bloch states and the more localized *d*-like orbitals of the cerium ion. The matrix elements describing the transitions originating from the 4*f* level to this region are sensitive to both the 5*d* and plane wave components. This is reflected by the $4f \rightarrow 5d$ resonances superimposed on the rising $4f \rightarrow$conduction-band absorption seen in Fig. 1. However, the ESA transition which originates from the lowest-5*d* orbital, is much less sensitive to these higher *d*-like states and the transition moment will be dominated by the dipole matrix elements between the lowest-5*d* orbital and the delocalized Bloch states.

Since the second 5*d* state overlaps the onset of the conduction band, optical pumping into this region can result in both the direct excitation of the cerium ions and the population of the electron trapping sites via the conduction band. Thus the ESA due to optically excited cerium ions would be observed simultaneously with other absorption processes involving these trap sites. This model for the multicomponent ESA is consistent with our measurements of the room-temperature ESA kinetics for 308-nm pumping and those by Jacobs *et al.*[1] for 350-nm pumping and Miniscalco[8] for 337-nm pumping. Since the lifetime of these transient color centers is governed by thermal excitation back into the conduction band, the decay rate of the absorption mediated by these color centers should be temperature dependent. The measurements by Owen *et al.*[3] at 77 K with 337-nm pumping of transient absorptions having 165-sec and 11-min decay components are indicative of this temperature dependent relaxation. Our observation of a 60% reduction in the time-integrated cerium fluorescence in the presence of a strong 680-nm probe pulse points to a competitive relaxation channel of the color centers which does not repopulate the cerium sites. This alternate relaxation mechanism is also expected to be temperature dependent.

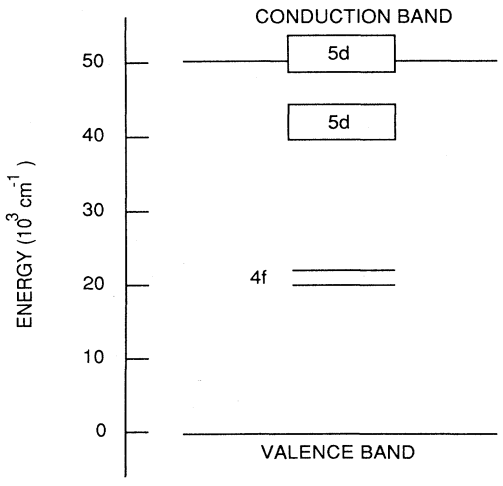

FIG. 7. Positions of the Ce^{3+} states relative to the conduction and valence bands of the YAG host.

The 337-nm and 350-nm pump wavelengths mentioned above are both below the photoionization threshold at 326 nm determined by Pedrini[4] and thus should not directly photoionize the cerium ions. Nevertheless, intense laser pumping into band-tail states can result in an appreciable number of photoionized cerium ions. The importance of these band-tail states is also evident from our observation of a significant photocurrent when the Ce:YAG sample is illuminated with the third harmonic of a Nd:YAG laser at 355 nm. Since the photoresponse was a linear function of the 355-nm photon flux, the photoconductivity is due to a single-photon transition at this wavelength.

There is undoubtedly a variety of different intrinsic electron traps with different energy gaps to the conduction band in Czochralski grown YAG. These different trap depths will be reflected in the multiple decay constants for both the optical absorption kinetics and the cerium afterglow for the shorter wavelength pumping. The existence of some very deep traps is suggested by our observation of a small but distinct background absorption which slowly grows in time with 308-nm pumping and then saturates at a steady-state value. These traps are also presumably important in the formation of a macroscopic, permanent dipole moment in our photoconductivity studies. Some of these defect sites have been identified[14] as oxygen vacancies, although the density and variety of these traps will be dependent on the crystal-growth technique and perhaps the impurity ion concentration.

The theoretical calculation of the spectral dependence of the ESA transition is frustrated by the incomplete knowledge of the YAG conduction bands and the appropriate crystal-field-mixed 5*d* wave functions as well as the role played by the lattice relaxation following the electronic transition. However, several general comments can be made. The shape of the absorption curve from a localized state in the gap to the conduction band will not necessarily resemble the valence-band to conduction-band transition with a simple energy shift. Furthermore, the localized state to band absorption has a strength and shape which is highly dependent on the characteristic volume of the initial-bound-state wave function.[15] If the characteristic radius of the localized initial-state wave function is a, then the overlap integral of this wave function and the plane-wave state with wave vector k will peak for those values of k such that $ka \approx 1$. Since the larger, momentum-band states lie at higher energy, the cross section of a localized state to band transition will peak at lower energies relative to the band edge for initial states with larger values of a. The 5*d* wave functions are much more diffuse than the 4*f* wave functions, and thus the 5*d* to conduction-band transition will have its maximum cross section at a significantly lower energy relative to the band edge than the 4*f* to

conduction-band absorption. Thus, although the low-energy threshold for photoionization transitions from excited states of impurity ions can be estimated from absorption and photoconductivity measurements from the ground state, there is not a simple way to predict the shape and peak positions for these ESA transitions.

VI. CONCLUSIONS

The Ce^{3+}:YAG crystal has many of the characteristics required for successful operation as a solid-state tunable laser. The emission band has a near-unity quantum efficiency at room temperature and extends from 500 to 650 nm. The broad pump bands have a dipole-allowed absorption. The YAG host has well-characterized thermal and optical characteristics. However, the strong ESA in this material precludes any net stimulated emission from the excited cerium ions. Our investigation of the ESA in Ce^{3+}:YAG has demonstrated that the conduction band of the host is the terminal state of the ESA which originates on the lowest-$5d$ state of the cerium ion. This assignment is consistent with both the magnitude and shape of the ESA spectrum. The threshold for the transition from the relaxed $5d$ state to the band edge is in agreement with that originating from the $4f$ ground state of the cerium ion. Using a strong probe beam to partially saturate the ESA transition, a slow and inefficient backflow of excitation to the cerium ions was observed. Thus the photoelectron does not always immediately return to the cerium hole site. The photoconductivity measurements were used to confirm the assignment of the terminal state of the ESA transition.

There is an important host dependent variation in the ESA of Ce^{3+}-doped crystals. These variations are expected to arise since the ESA spectrum in these materials will depend on the location of the excited Ce^{3+} states within the band gap of the host. In Ce^{3+}:CaF_2 and Ce^{3+}:$YLiF_4$, an ESA occurs at the wavelength of the near-uv pump bands.[16,17] These ESA transitions also terminate in the host conduction band. Color centers formed following the photoionization of the cerium ions diminish the laser potential of both of these cerium-doped fluoride crystals. In Ce^{3+}:YAG, a strong ESA occurs at much longer wavelengths which overlap the emission bands of the Ce^{3+} ions. Thus the ESA in this crystal directly quenches the stimulated emission and prevents the buildup of any optical gain.

These results may have important implications for other potential solid-state laser materials. Even when the higher-lying energy states of the dopant ion are absent or have low transition cross sections from the laser level, photoionization transitions to the host conduction band may still degrade or inhibit laser operation in the material. The strength and spectral position of these ESA transitions to the conduction band cannot be determined directly from ground-state absorption measurements.

ACKNOWLEDGMENTS

This research was performed under the auspices of the Division of Material Sciences of the Office of Basic Energy Sciences, United States Department of Energy, under Grant No. DE-FG02-84ER45056.

APPENDIX: BEAM OVERLAP INTEGRAL

The overlap integral of the pump and probe transverse profiles, defined by Eq. (5), can be evaluated analytically for a number of assumed profile functions. One case of practical interest is two concentric Gaussian functions. If the $1/e$ radii of the probe- and pump-beam Gaussian profiles are r and R, respectively, then the overlap integral can easily be found to be

$$W=[\pi R^2(1+r^2/R^2)]^{-1} . \tag{A1}$$

The value of W is seen to be approximately one over the transverse area of the pump beam. Although the beam profiles for both dye lasers were roughly Gaussian-shaped functions, the value of W is as much dependent on the details of the actual beam shapes as on their characteristic dimensions. To find a better estimate for the overlap integral, we have measured the beam profile and completed the integration numerically. The profiles were measured by scanning a razor blade across the beams at the position of the sample in both the vertical and horizontal directions. The pump-beam energy passing the aperture was measured at 50-μ intervals and is related to the pump beam transverse profile by

$$A(x_i)=\int_{-\infty}^{x_i}\int_{-\infty}^{\infty} J(x,y)\,dx\,dy , \tag{A2}$$

$$B(y_j)=\int_{-\infty}^{\infty}\int_{-\infty}^{y_j} J(x,y)\,dx\,dy , \tag{A3}$$

with similar expressions for the probe beam. The scans were interpolated using a cubic-spline fit at 25-μm intervals and then numerically differentiated with respect to the x or y coordinates. We have assumed that the probe and pump profiles can be written as products of these derivative functions, i.e.,

$$j(x_i,y_j)=g(x_i)h(y_j) , \tag{A4}$$

$$J(x_i,y_j)=G(x_i)H(y_j) , \tag{A5}$$

and that they have been properly normalized so that,

$$1=\sum_{ij} g(x_i)h(y_j)\Delta x_i \Delta y_j , \tag{A6}$$

$$1=\sum_{ij} G(x_i)H(y_j)\Delta x_i \Delta y_j . \tag{A7}$$

The overlap integral is then estimated from the sum

$$W=\sum_{ij} g(x_i)h(y_j)G(x_i)H(y_j)\Delta x_i \Delta y_j . \tag{A8}$$

These numerical procedures were used to evaluate the overlap integral for a variety of different pump- and probe-beam spot sizes. The cross sections that were derived for these different geometries had a variance of about 30% from the mean values that are quoted in the text.

*Present address: Department of Physics and Engineering Physics, Stevens Institute of Technology, Hoboken, NJ 07030.
†Present address: Department of Physics, Southern Illinois University, Edwardsville, IL 62026.
‡Present address: Analysis & Technology, Inc., North Stonington, CT 06359.

[1]R. R. Jacobs, W. F. Krupke, and M. J. Weber, Appl. Phys. Lett. **33**, 410 (1978).
[2]W. J. Miniscalco, J. M. Pellegrino, and W. M. Yen, J. Appl. Phys. **49**, 6109 (1978).
[3]J. F. Owen, P. B. Dorain, and T. Kobaysi, J. Appl. Phys. **52**, 1216 (1981).
[4]C. Pedrini, F. Rogemond, and D. S. McClure, J. Appl. Phys. **59**, 1196 (1986).
[5]R. S. Van Heyningen and F. C. Brown, Phys. Rev. **111**, 462 (1958).
[6]Ronald D. Ghen, Masters thesis, University of Connecticut, 1986.
[7]M. J. Weber, Solid State Commun. **12**, 741 (1973).
[8]W. J. Miniscalco (unpublished).
[9]C. M. Wong, S. R. Rotman, and C. Warde, Appl. Phys. Lett. **44**, 1038 (1984).
[10]D. S. Hamilton, in *Tunable Solid State Lasers,* edited by P. Hammerling, A. B. Budgor, and A. Pinto (Springer-Verlag, Berlin, 1985).
[11]D. J. Robbins, J. Electrochem. Soc. **126**, 1550 (1979).
[12]D. J. Robbins, B. Cockayne, J. L. Glasper, and B. Lent, J. Electrochem. Soc. **126**, 1213 (1979).
[13]G. A. Slack, D. W. Oliver, R. M. Chrenko, and S. Roberts, Phys. Rev. **177**, 1308 (1969).
[14]K. Mori, Phys. Status Solidi A **42**, 375 (1975).
[15]B. K. Ridley, *Quantum Processes in Semiconductors* (Oxford, New York, 1982).
[16]G. J. Pogatshnik and D. S. Hamilton, Phys. Rev. B **36**, 8251 (1987).
[17]Ki-Soo Lim and D. S. Hamilton, J. Lumin. **40&41**, 319 (1988); J. Opt. Soc. Am. B (to be published); Ki-Soo Lim, Ph.D. thesis, University of Connecticut, 1987.